Heliostat aiming point optimization for external tower receiver

Marco Astolfi *, Marco Binotti, Simone Mazzola, Luca Zanellato, Giampaolo Manzolini

Group of Energy Conversion Systems (GECOS), Politecnico di Milano, Dipartimento di Energia, Via Lambruschini 4, 20156 Milano, Italy

Received 19 June 2015; received in revised form 3 March 2016; accepted 20 March 2016
Available online 18 April 2016

Communicated by: Associate Editor Lorin Vant-Hull

Abstract

Reduction of peak fluxes on solar receiver is an important research topic because peak minimization can lead to lower receiver tem-peratures with advantages in terms of thermal efficiency and mechanical stresses. This work proposes different approaches for the min-imization of the heat flux on external tower receiver with surround field. The mathematical formulation is implemented in Matlab, while Delsol is used for the heliostat field modeling. Since the number of variables is very high, branching the original optimization problem in a set of sub-problems is a beneficial technique. Four approaches, based on this concept, are here proposed: they differ for the number of field sectors considered in the optimization process and on the heliostat projection modeling. The best approach, which considers the overlapping effect between adjacent sectors, can reduce the peak flux down to 770 kW/m^2 in 120 s of computational time. This value is about 15% lower than reference aiming strategies available in literature. The optimized flux is almost flat in the central part of the receiver while it has significant gradient at the lower and upper border. Finally, a sensitivity analysis shows that the proposed approaches work well at any given solar position and with different heliostat assumptions (i.e. curvature and errors).

Keywords: Heliostat aiming point; Spillage losses; Yearly optical efficiency; Solar tower plants

1. Introduction

In the last years, renewable energy sources faced a significant growth to reduce the fossil fuels usage, to increase the supply and the diversification in the power generation sector. Among renewable sources, solar energy together with wind energy showed the most relevant increase (IEA, 2011; REN21, 2013) thanks to its abundant avail-ability. Main drawbacks are the low flux density (with a maximum of about 1 kW/m^2) and limited conversion efficiencies (Wright et al., 2000).

Concentrated solar power (CSP) attempts to overcome these limitations by concentrating the solar radiation onto a receiver where the heat is transferred to a fluid (typically at high temperature), then used in a conventional power cycle. One of the main advantages of CSP over photovoltaic is the capability of storing the thermal energy in a storage system, at a reasonable cost, decoupling the solar source from the electric power production (the so-called dispatchability (Alliance, 2012)). Currently, the main disadvantage of CSP with respect to photovoltaic is the higher Cost of Electricity (COE) as consequence of the higher installation cost (SunShot website, 2014).[1]

* Corresponding author.
URL: http://www.energia.polimi.it (M. Astolfi).

[1] However, the calculated COE for CSP includes storage, which is not taken into account in PV systems: the extra-value of dispatchability has been quantified between 6.6 and 16.7 $/MW h, depending on case-specific features (Delhom and Hommon, 2012). Nevertheless, it is clear that CSP cost reduction is necessary to become competitive against both other renewables and fossil fuel power technologies.

Published Journal Article available at: http://dx.doi.org/10.1016/j.solener.2016.03.042

Nomenclature

α	y-coordinate of the aiming point (m)
A	overall area of the heliostats (m^2)
γ	Azimuth angle (°)
ϑ	angle of receiver/field sector (°)
θ_z	Zenith angle (°)
η	optical efficiency (%)
I	peak flux intensity (kW/m^2)
Q	thermal heat flux on the receiver (kW/m^2)
R	slant range (km)
σ	Gaussian variance
y	vertical distance from the receiver center (m)
φ	heat flux entailed by one heliostat

Subscripts/superscripts

el	electrical
ϑ	angle of receiver sector
i	generic heliostat or approach
y	vertical distance from receiver center

Acronyms

COE	cost of electricity
CSP	concentrated solar power
DAPS	Dynamic Aim Processing System
DNI	Direct Normal Irradiance
EO	Explicit Overlap Optimization
OF	objective function
OOEA	overall optimization with empirical approach
PSSO	Progressive Single Sector Optimization
PV	Photovoltaic
SAPS	Static Aim Processing System
STZ	Standard Time Zone
S-G	Sanchèz-Gonzalez

Solar tower plants are regarded as the CSP technology with the highest cost reduction potential. Nonetheless, although this concept was firstly tested in the early eighties (Behar et al., 2013; Delaquil et al., 1991), the number of commercial plants in the world is still limited, though increasing. Nowadays, about 450 MW_{el} total installed capacity of commercial power tower plant are operational mainly in Spain (PS10, 11 MW (Solucar, 2006), PS20, 20 MW, and Gemasolar, 20 MW (Gemasolar, 2014)) and in US ((Ivanpah plant, 2014), 377 MW), while other 450 MW_{el} are under construction worldwide in South Africa (Khi Solar One thermal power plant, 50 MW (Abengoa, 2014)), in Chile (Planta Solar Cerro Dominador, two plants 110 MW each), in China (Delingha Supcon Tower Plant, 50 MW) and US (Crescent Dunes, 110 MW). In addition, more than 3 GW_{el} are under construction or planned (CSP world website, 2014).

This work investigates the adoption of optimized heliostats aiming strategies for the reduction of peak energy fluxes on the tower receiver that might lead to potential cost reduction thanks to a new design process (Boerema et al., 2013). Solar Two power tower used Static Aim Pro-cessing System (SAPS) to adjust heliostat aim points every ten minutes during normal operation, while a Dynamic Aim Processing System (DAPS) protects the receiver from overflux conditions by comparing the predicted receiver flux pattern against allowable flux limits (Pacheco, 2002). Gemasolar plant takes advantage of the software SENSOL, which is characterized by a performance simulation model fine-tuned with real plants in commercial operation (Sener, 2014).

Several works have dealt with heliostat field optimization (Buck and Teufel, 2009; Collado and Guallar, 2013; Collado, 2009; Garcia et al., 2008; Landman and Gauché, 2014; Lipps et al., 1985; Vant-Hull and Izygon, 2003; Rodríguez-Sánchez et al., 2014a,b; Sanchez and Romero, 2006; Vant-Hull et al., 1996), and some of these focus on peak flux reduction on solar receivers. Vant-Hull et al. (1996) made the first study available in literature, developing an innovative aiming strategy with adjusted aim level for each region. GarcÍa-MartÍn et al. (1999) pro-posed a closed loop control method for CESA-1 project. Each individual heliostat is pointed to one of the five aim-ing point according to the temperature distribution mea-sured by thermocouples, in order to avoid temperature peaks. The method proposed is relevant and successful, but it is not based on an optimization process. (Salomé et al., 2013) proposes an open-loop control strategy to con-trol the flux distribution on the surface of a flat plate recei-ver. Results show that the most important parameters for peak flux reduction are the receiver size (i.e. concentration ratio) as well as the number of the considered aiming points. (Besarati et al., 2014) proposed a new optimization approach based on the principles of Genetic Algorithm for a flat plate receiver, calculating the flux density again with HFCAL, while (Yu et al., 2014) developed a non-central focal model based on the Monte-Carlo Ray-Tracing method. (G. Augsburger, 2013) proposed two novel aiming strategies for external cylindrical receivers: distance-based and deviation-based. In the former, the heliostats point at different positions along the vertical coordinate of the receiver surface according to their distance from the tower base, while in the latter the pointing criterion is related to the calculated optical deviation from the target. The deviation-based strategy guarantees a better decrease of heat flux peak and maximum gradient, with lower impact on the total incident power.

Unlike the case of the flat plate receiver, only three works in literature deal with the definition of an aiming strategy for a surround field (Rodríguez-Sánchez et al., 2014a,b;

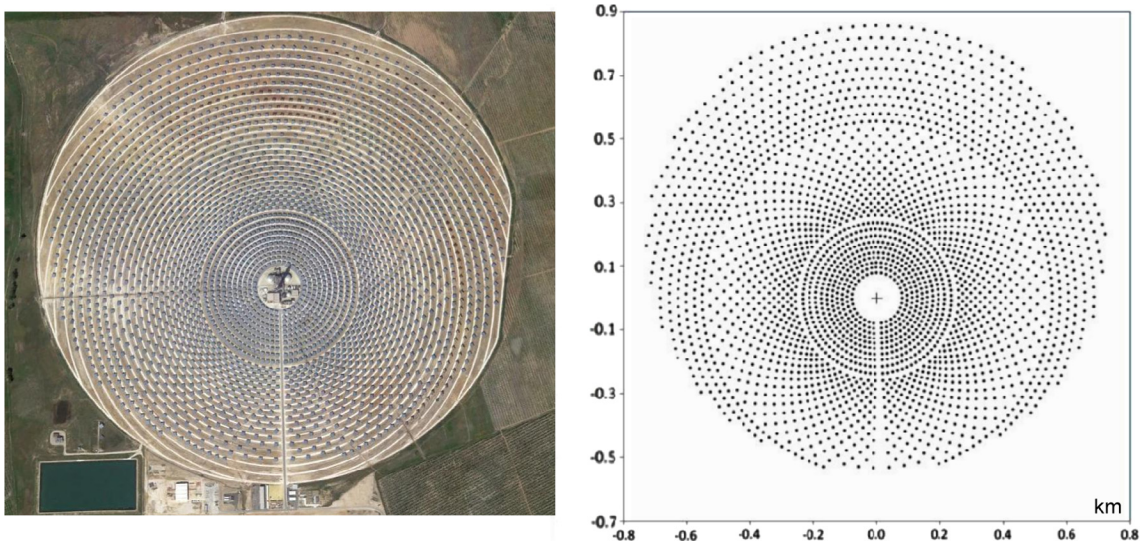

Fig. 1. Satellite picture of Gemasolar plant (Google Earth snapshot) and its implementation in Delsol.

Sánchez-González and Santana, 2015a; Vant-Hull et al., 1996). Among these three works, the latest is described in detail in the next section and will be used as term of comparison for the approaches developed in this study.

The objective of this work is the definition of new aiming strategies through different optimization tools in order to improve the tracking management.

The strategies are applied to an external receiver with surround field which is the most complex case (i.e. highest number of heliostats).

Since the aim of the work is the optimization of the aiming strategy, the optical tool for the optimization should perform the assessment in a short time. Among the available approaches used to obtain the heat flux distribution on a solar receiver, the analytical approach is preferred with respect to the Monte Carlo's one. In the former, the reflected image from each mirror is considered with its error cones calculated by convolutions of normal Gaussian distributions corresponding to each error (sun shape and heliostat errors). Previous studies showed that the differences between the peak flux and optical efficiency obtained with the two approaches are in the order of 1–2%, and reduce for larger plant size (Garcia et al., 2008). Among the available optical tools based on convolutions, DEL-SOL3 is selected (Delsol web page, 2014; Kistler, 1986).

The paper is organized as follows: the case study and reference aiming point approaches are presented, then the approximation through Gaussian is introduced. Afterwards, the description of optimization approaches based on single or multi-sector are discussed. Finally, results in terms of peak fluxes and computational efforts are discussed outlining advantages and disadvantages of each approach.

2. Case study

The different aiming strategies and optimization approaches studied in this work are applied to a Gemasolar type solar plant (Gemasolar, 2014).

Gemasolar plant has a surround field and an external cylindrical receiver where molten salts are heated from 290 °C to 565 °C. The lowest temperature faces the north side of the field (i.e. highest peak fluxes), while the highest temperature coincides with the south side. The heliostat field is reported in Fig. 1 and the main assumptions about the receiver and the heliostat field are summarized in Table 1. The impact of some assumptions on the results will be evaluated through a sensitivity analysis.

All the optimizations are performed at solar noon on the summer solstice (21st June, sun position ($\theta = 14.12°$, $\gamma = 0$).) in Seville, Spain (Latitude = 37.56°, Longitude = 5.33°, STZ = 1) assuming a clear sky condition, a Direct Normal Irradiance (DNI) of 991 W/m2. The condition was selected since it is one with the highest incidence power along the year.

It must be outlined that the formulation of the proposed strategies is general and it can be applied at any time of the year as shown in the results section.

The heliostat field and the receiver are divided in sectors and vertical lines respectively, which are both described by the ϑ angle (positive clockwise and negative anticlockwise). The sector $\vartheta = 0°$ is assumed to be in the opposite position of the sun with respect to the solar tower. In Fig. 2, it is represented the solar field division in 31 sectors so that each one has one mirror in the first radial zone, and 38 radial zones for a total of 1178 zones. The division is carried out assuming a circular field, therefore 148 zones do not contain any heliostat (i.e. the south part of the field). In the following approaches it is assumed that all the helio-stats in a radial zone point at the same y coordinate on the receiver facing vertical line. Aiming on a different receiver vertical line is generally detrimental since it often results in an increase of both receiver cosine losses and spillage losses.

Finally, some indicators adopted in this work to compare all the investigated cases are here reported: the considered indicators are the optical efficiency, the peak flux, the

Table 1
Sun and tower system assumptions.

Day	21st of June
Site longitude	5.33°W
Site latitude	37.56°N
DNI (W/m^2)	991, clear sky
Sun position	$\gamma = 0°$, $\theta = 14.12°$
Receiver size	
Height (m)	16
Diameter (m)	8
Tower height (m)	134
Field type	Surround
Minimum radius of the field (m)	78.89
Maximum radius of the field (m)	880
Number of heliostats	2650
Heliostat size (m × m)	11 × 10
Heliostat type	Single facet with focal curvature
Focus (km)	Slant range (R)
Mirror reflectivity	0.93
Attenuation	$100 - (0.6739 + 10.46 \cdot R - 1.70 \cdot R^2 + 0.2845 \cdot R^3)$
Heliostat Errors (mrad)	
Heliostat angles	0.75
Surface normal	1.0
Reflected vector	2.9
Curvature	Spherical
Sun shape	Limb Darkened Sun (NSUN = 1) (Ho, 2008; Kistler, 1986)

spillage and the spillage variation. The optical efficiency (η) is the ratio between the energy on the receiver ($\dot{Q}_{receiver}$) and the maximum solar irradiation available.

$$\eta = \frac{\dot{Q}_{receiver}}{\mathrm{DNI}\ A} \tag{1}$$

where A is the overall area of the heliostats.

The optical losses include cosine, shadowing, blocking, mirror reflectivity, blocking, air attenuation and spillage. The receiver absorptivity is not included in the optical efficiency.

Among the losses, the heliostats aim point variation affects only the spillage which is the amount of energy directed toward the receiver which does not hit the absorbing area (Eq. (2)). The spillage variation compared to the reference case is determined as shown in Eq. (3).

$$Spillage = 1 - \frac{\dot{Q}_{receiver}}{\dot{Q}_{reflected}} \tag{2}$$

$$\Delta Spillage(\%) = Spillage_{reference} - Spillage_{i-approach} \tag{3}$$

3. Reference aiming point approaches

Two different aiming point approaches are here defined and will be used as terms of comparison to evaluate the innovative strategies in this work. The first one, named REF, is the most simple and intuitive: it consists of pointing each heliostat toward the equator of the receiver. It ensures that the spillage losses are the lowest feasible but it entails a high non-uniformity of the heat flux, as shown in Fig. 3. In our case study, the heat flux has very high val-ues reaching the peak value of 2140 kW/m^2 on the northern side of the receiver. [2]

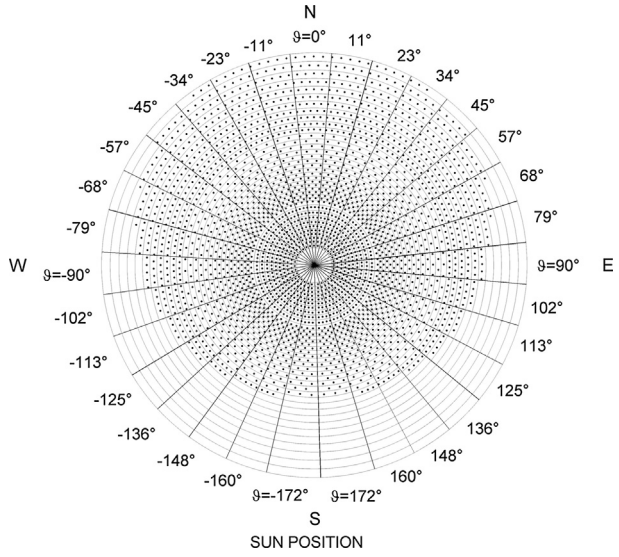

Fig. 2. Solar field divided in 31 sectors and 38 radial zones.

The second strategy is based on Sanchez-Gonzalez approach, named S-G, (Sánchez-González and Santana, 2015b) and is similar to the ones proposed by (Augsburger and Favrat, 2013; Lipps and Vant-Hull, 1978). In this approach, the aim point of each heliostat is set to have the projection image tangent to one of the recei-ver edges. This ensures that a relevant part of the heat flux is shifted away from the middle, while keeping the spillage losses under control. As shown in Fig. 3, this approach makes the flux more uniform reducing the peak down to 896 kW/m^2 (i.e. 58% lower than the REF flux). As draw-back, the spillage slightly increases by 0.2% (i.e. 6.3% vs 6.1% of the REF case). However, the resulting heat flux is not fully optimized as indicated by the two symmetric peaks on the receiver.

Finally, the ideal flux on the receiver can also be determined assuming the same incidence power of the single aiming strategy uniformly spread along the height of the receiver. In other words, the ideal heat flux for a given sector is the average value of the single aim strategy heat flux. This condition is not practically implementable since it requires an infinite number of very small heliostats and the sun as point source but it can be effectively used as reference benchmark for our purposes. According to this

[2] Pointing all the mirrors to the equator of the receiver is one of the possible aiming strategies that can be taken as reference. In particular, for the heliostats nearby the tower base may be better to point slightly lower than the receiver equator to reduce the spillage in vertical direction due to sun image elongation. Different aiming strategies would result in different Spillage reference values but they will not affect the final results obtained in this work.

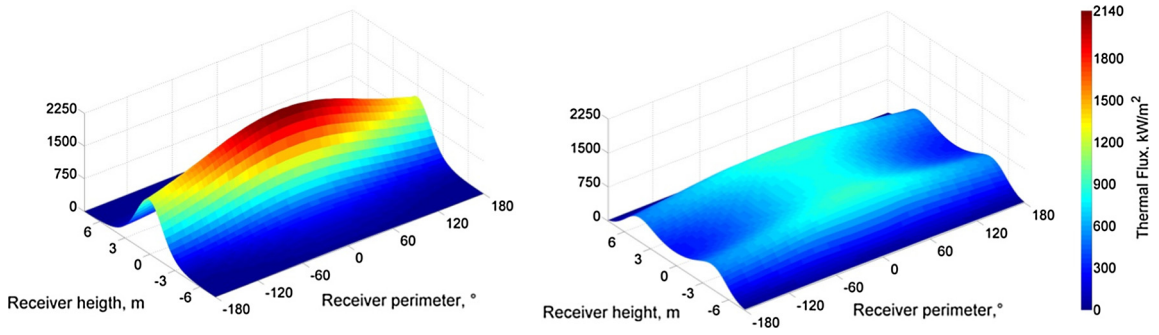

Fig. 3. Flux on the Gemasolar receiver panels obtained with single aim-REF strategy (left side) and with a multi-aiming strategy based on S-G (Sánchez-González and Santana, 2015b) (right side).

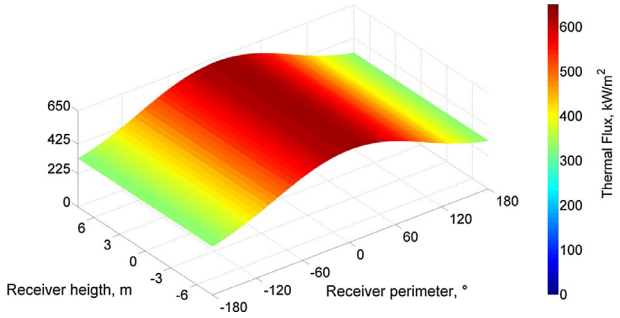

Fig. 4. Ideal flux map on the receiver.

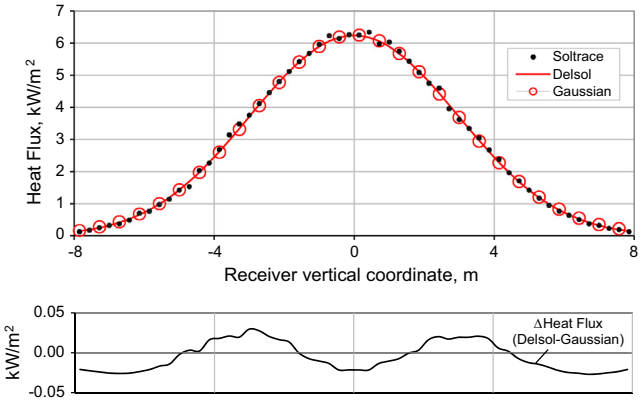

Fig. 5. Heat flux profile on the 0° receiver vertical line produced by four heliostats aiming at the center of the receiver. Results obtained with SolTrace and Delsol are compared; the best-fit Gaussian curve is also reported (Gaussian approximation). The difference between Delsol and the best-fit Gaussian curve is reported in the bottom figure.

definition, the ideal heat flux map of the whole receiver is shown in Fig. 4 with a peak of 625 W/m^2 (70% and 30% lower than the REF and S-G strategies respectively). This ideal map will be used in the mathematical formulation of the problem as it will be explained later.

For the selected heliostat field, it is impossible to achieve a uniform flux along the perimeter of the receiver even in the ideal case because the heliostats are not homogenously distributed along the field and because the heat flux depends on the heliostat position in the field with respect to the sun position (i.e. beam incidence angle).

4. Gaussian approximation

In order to limit the computational time, a simplified method to describe the heat flux onto the receiver, called "Gaussian approximation", is introduced and will be used in most of the proposed optimization approaches discussed in the following paragraphs.

It consists of describing the flux profile on the receiver by Gaussian curves (one for each sector of the solar field) which best fit the Delsol output flux with the least square method. This approach can be applied to both single heliostat and group of heliostats. The Gaussian approximation is based on the consideration that the only parameter of influence on the receiver flux distribution is the heliostat vertical aim point. The heat flux intensity along the receiver vertical line is thus described by the generic Gaussian function:

$$\varphi_y = I \cdot \exp\left(-\frac{y^2}{2\sigma^2}\right) \tag{4}$$

where y is the vertical distance from the center of the receiver, I is the peak flux intensity and σ^2 is the Gaussian variance. In Fig. 5, the comparison between the heat flux calculated with a raytracing tool (Soltrace), with Delsol and the corresponding best-fit Gaussian curve, produced on a receiver vertical line by a group of heliostats is reported.

The Gaussian Approximation curve can be adopted within the optimization process only if the heliostats projection does not change significantly when varying the aim point of a heliostat along the facing receiver vertical line. From this point of view the most critical heliostats are the ones closest to the tower base, since their distance from the receiver is the minimum and thus the impact on the flux shape is maximum. Table 2, reports the best-fit Gaussian curve parameters variation along with vertical aim point variation (±4 m) for the four heliostats closest to the tower in the four cardinal directions: results show that the variation in terms of I and σ are limited, justifying the use of a Gaussian curve with the same parameters

Table 2
maximum variation of Intensity and Variance of the heat flux best-fit Gaussian curve with the variation of the aim point from $y = -4$ (bottom of the receiver) to $y = 4$ (top of the receiver). The variation is reported with respect to the mean value and for the four heliostats closer at the tower base in the four cardinal directions. Differences between East and West sectors values are different because of not perfect symmetry of the solar field.

	North	East	South	West
ΔI (%)	10^{-3}	10^{-3}	10^{-3}	10^{-3}
$\Delta\sigma^2$ (%)	0.077	−0.255	0.045	0.033

(I, σ^2) but centered on a different mean value, corresponding to the aim point (α).

Eq. (4) thus becomes:

$$\varphi_y = I \cdot \exp\left(-\frac{(y-\alpha)^2}{2\sigma^2}\right) \tag{5}$$

The Gaussian approximation is adopted in this study because the optimization of the heat flux onto the receiver generally needs a large number of iterations. A pre-processing stage to collect all the information for the Gaussian curves is required, but then the optimization could be performed without running Delsol with a relevant reduction of the overall computational time. The heat flux coming from each heliostat or group of heliostats on the corresponding receiver portion is determined by pointing the selected heliostats to the equator of the receiver and numerical data are interpolated with 1-D Gaussian functions. Each aiming strategy needs a different number of Delsol simulations as it will be discussed in each section.[3]

5. Novel aiming strategies

In this section, the proposed optimization methods are discussed; each one aims at reducing the peak flux and at obtaining a uniform heat flux map on the solar tower receiver. The objective function (OF) to be minimized is the sum of the differences between the maximum flux calculated on a receiver vertical line and the corresponding ideal flux for that receiver portion. Consequently, the problem OF can be written as follows:

$$\mathrm{OF} = \sum_{\vartheta\in[-\pi,\pi]} \left(\max(Q_{\vartheta,y} - \overline{Q}_{\vartheta})\right) \tag{6}$$

where $Q_{\vartheta,y}$ (kW/m^2) is the heat flux on the receiver in the point (ϑ, y) and $\overline{Q_{\vartheta}}$(kW/m^2) is the ideal value of the flux on the ϑ receiver strip (see Fig. 4).

Note that, for a given ϑ, the difference ($Q_{\vartheta,y} - \overline{Q}_{\vartheta}$) could be negative for some points, but the maximum along the vertical line is always positive if a maximum spillage constraint is considered (see Eq. (9)).

The punctual heat flux ($Q_{\vartheta,y}$) is equal to the sum of the effects of all the heliostats having influence on a certain receiver point (see Eq. (7)). The effect of each i-th radial zone is described by a Gaussian function ($\varphi^i_{\vartheta,y}$ (kW/m^2)) which is a function of its aiming point (α^i[m]) (see Eq. (8)).

$$Q_{\vartheta,y} = \sum_i \varphi^i_{\vartheta,y} \tag{7}$$

$$\varphi^i_{\vartheta,y} = f(\alpha^i) \tag{8}$$

Finally, a global constraint is added to the problem in order to keep under control the spillage losses:

$$\Delta\mathrm{Spillage} \leqslant \overline{\Delta\mathrm{Spillage}} \tag{9}$$

where ΔSpillage is the actual spillage variation obtained upon defining the aiming points of each heliostat and $\overline{\Delta\mathrm{Spillage}}$ is the imposed upper bound. The resulting optimization problem has a very high complexity if compared to the cavity receiver case (Salomé et al., 2013). The number of variables, i.e. the number of heliostats groups (namely the 1030 radial zones containing heliostats), is very high and the approaches here proposed will split the main problem into a sets of simpler sub-problems.

5.1. Single-sector optimization (SSO)

The first approach consists in dividing the problem in 31 sub-problems, one for each radial sector of the solar field. The maximum heat flux on each receiver vertical line is minimized considering only the heliostats in the facing solar field sector and neglecting the overlap effect of neighbor ones. Thanks to this assumption, the number of optimization variables is reduced to 38 (the number of radial zones of the $\vartheta = 0°$ sector) and each sub-problem can be solved rapidly and efficiently by basic optimization algorithms available in Matlab.[4] The pre-processing stage requires 1030 Delsol simulations to obtain the heat flux profile from each radial zone of the solar field on the facing receiver vertical line.

In Fig. 6, the flux on the $\vartheta = 0°$ receiver vertical line resulting by the optimization pointing of the facing sector is compared to the flux attainable with a single aim strategy namely pointing all the heliostats to the equator of the receiver (REF case). A relevant reduction of the maximum heat flux can be achieved with a final flux profile close to a pillbox with a trend almost flat in most of the receiver vertical line. Results are presented only for the $\vartheta = 0°$ sector since it has the highest heat flux, but similar result can be addressed for all the other sectors.

In this strategy, the optimization was carried out neglecting the overlap effects of neighbor sectors. This

[3] Considering that Delsol software has a limit of 169 grid points on the receiver and the necessity to accurately describe the heat flux on the receiver, for each Delsol simulation it is possible to evaluate only the heat flux from one radial zone on a single receiver vertical line.

[4] Different optimization algorithms have been tested (Genetic Algorithm, Fmincon, PatternSearch); for this optimization, the fastest and most stable have been Fmincon with Interior Point method.

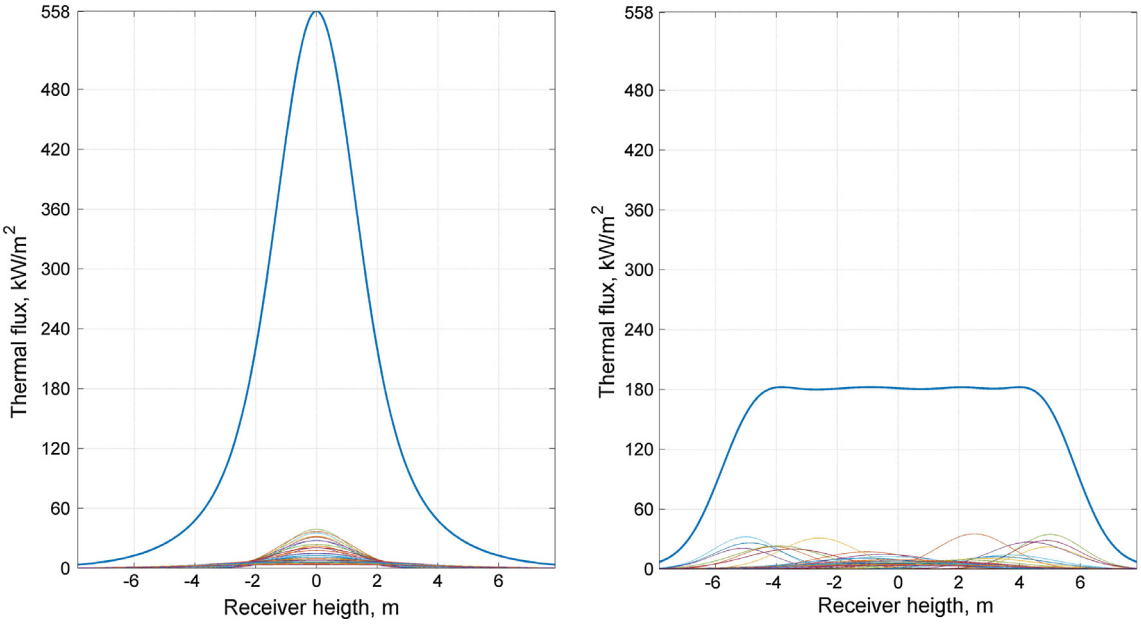

Fig. 6. Flux profile on the $\vartheta = 0°$ vertical line, base case and optimized strategy, no spillage variations.

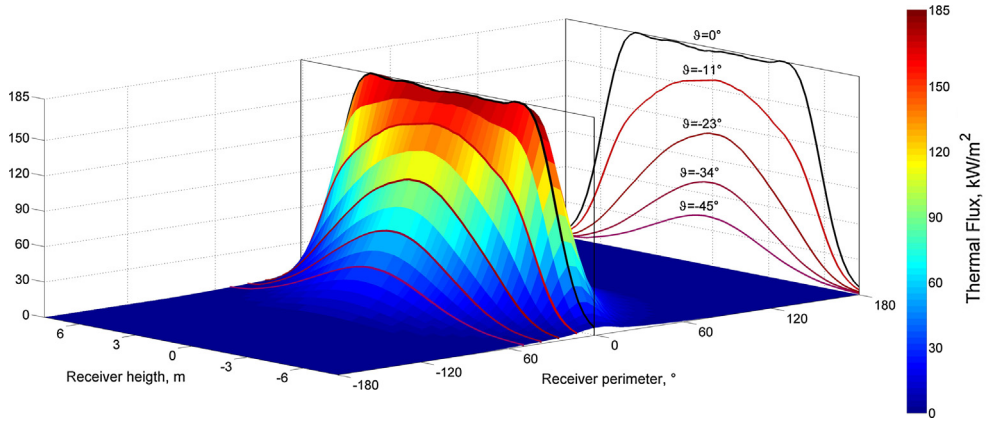

Fig. 7. Flux contour calculated in Delsol with the optimized aiming strategy for total flux coming from $\vartheta = 0°$ sector. The black line represent the heat flux profile on the $\vartheta = 0°$ receiver line while red lines represent the cross effect on the adjacent receiver portions, $\vartheta = \pm 50°$. (For interpretation of the references to colour in this figure legend, the reader is referred to the web version of this article.)

assumption can be adopted only for perfectly square heat flux profiles in both vertical (y) and circumferential (ϑ) direction; a condition that cannot be achieved. The heat flux presents a steep trend at the extremity of the receiver considered in the optimization while on the circumferential direction, the gradients are less marked and the flux on the adjacent receiver lines is closer to a Gaussian function than to a pillbox (see Fig. 7).

This is due to the heliostats in farthest radial zones which have a large solar image and they must point to the equator of the receiver in order to limit the spillage losses.

Applying the same procedure to the entire solar field and then considering the cross effects of the adjacent sec-tors, an optimized heat flux profile with a significant peak is obtained (see Fig. 8) because of the overlapping effect of neighbor sectors, which was neglected in the optimiza-tion process. As reported in Fig. 8, for $\vartheta = 0°$ sector, only 22% of the total thermal flux comes from the facing solar field sector and sectors up to $\vartheta = \pm 30°$ have a relevant contribution on the total heat flux.

This strategy allows reducing the maximum heat flux with respect to the reference, but the Sanchez Gonzales strategy leads to a better result even if it does not directly account for the overlap effects.

Two main observations can be addressed considering the results achieved with this aiming strategy: (i) it is possible to efficiently flatten the heat flux on a single strip by acting on the aiming of 38 radial zones hence the size of the problem can be easily handled by stable and fast numerical algorithms, (ii) the overlap of neighbor heliostats fluxes cannot be neglected in the problem definition since it strongly distorts the heat flux profile on each receiver vertical line. These considerations are taken into account in the following strategies.

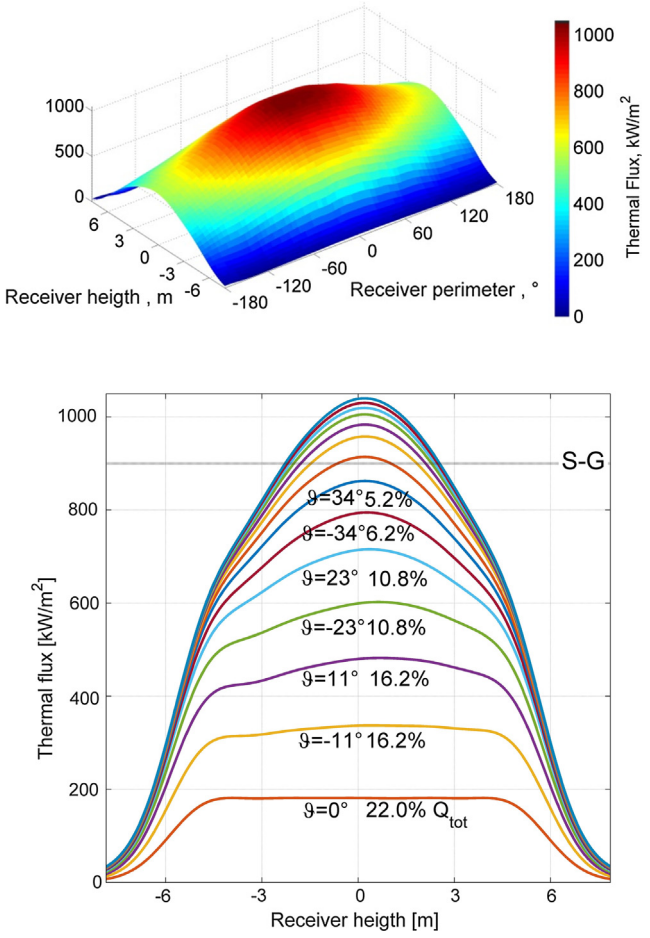

Fig. 8. Results obtained with SSO aiming strategy: (top) overall flux map obtained with SSO and (bottom) Flux profile on the $\vartheta = 0°$ receiver vertical line (the contribution of the different sectors is reported in a stacked diagram).

5.2. *Progressive-single-sector optimization (PSSO)*

This approach analyses all the sectors following a predefined order and it optimizes for each one the *y*-pointing of the 38 radial zones on the facing receiver vertical line. Before starting each optimization, the effect of the previously analyzed sectors on the present receiver vertical line is computed in Delsol: this heat flux is imposed as a base profile for the optimization. Differently from the previous strategy, this optimization algorithm takes into account the information about the overlap effects of the previously optimized sectors; for example in the optimization of the *n*th receiver line the heat flux of the *n*th−1 sectors already optimized is considered as a base heat flux.

The order followed in the sectors optimization obviously affects the results and several criteria were attempted. Two of the most promising ones are reported in Fig. 9a and b. The pre-processing stage is common to both strategies and it requires 1030 Delsol simulations equal to the num-ber of radial zones in the solar field.

The first approach (PSSO1) starts optimizing sector $\vartheta = -174°$ with a single sector approach. All the other sec-tors are then optimized one by one moving toward $\vartheta = 0°$ with the scheme reported in Fig. 9a and the code takes into account more and more information about the influence of the neighbor sectors while completing the analysis of the entire solar field. As result, it can flatten the peak of heat flux in the last sector where the conditions are more critical, but it pays for a less homogeneous flux in the other sectors compared to the previous approach. This approach requires 31 single-sector optimizations and 30 Delsol simulations.

The second approach (PSSO2) requires two steps. $\vartheta = \pm 90°$In step one, half of the sectors (16) are optimized independently with the single-sector strategy without considering the cross effects. For each one a heat flux close to a pillbox is obtained in vertical direction. At step two, the remaining sectors (15) are optimized one by one start-ing from the sector $\vartheta = +158°$ (which is the less critical one) and moving toward $\vartheta = 0°$ following the order in Fig. 9b All the sectors optimized in step two consider the overlap effect of the neighbor sectors already analyzed. The analysis of the whole solar field requires 31 single sec-tor optimizations and 14 Delsol simulations.

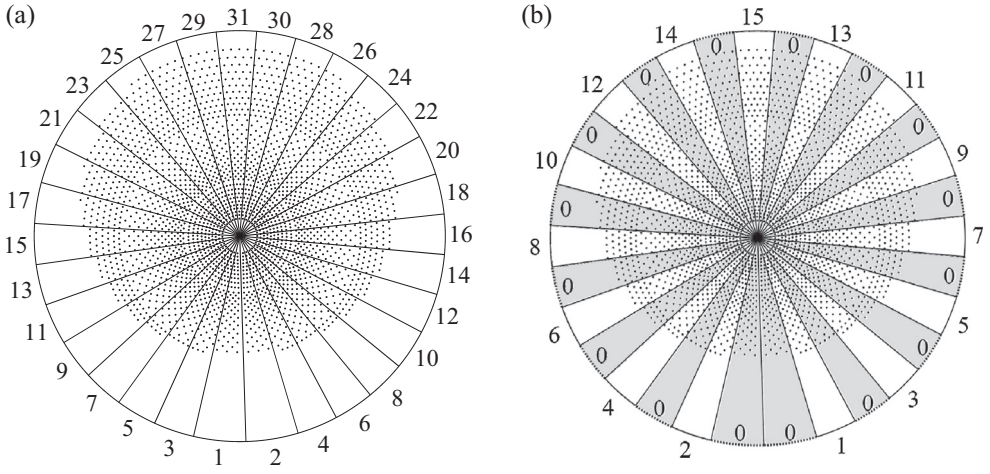

Fig. 9. Representation of the two orders followed in PSSO1 (a) and PSSO2 (b).

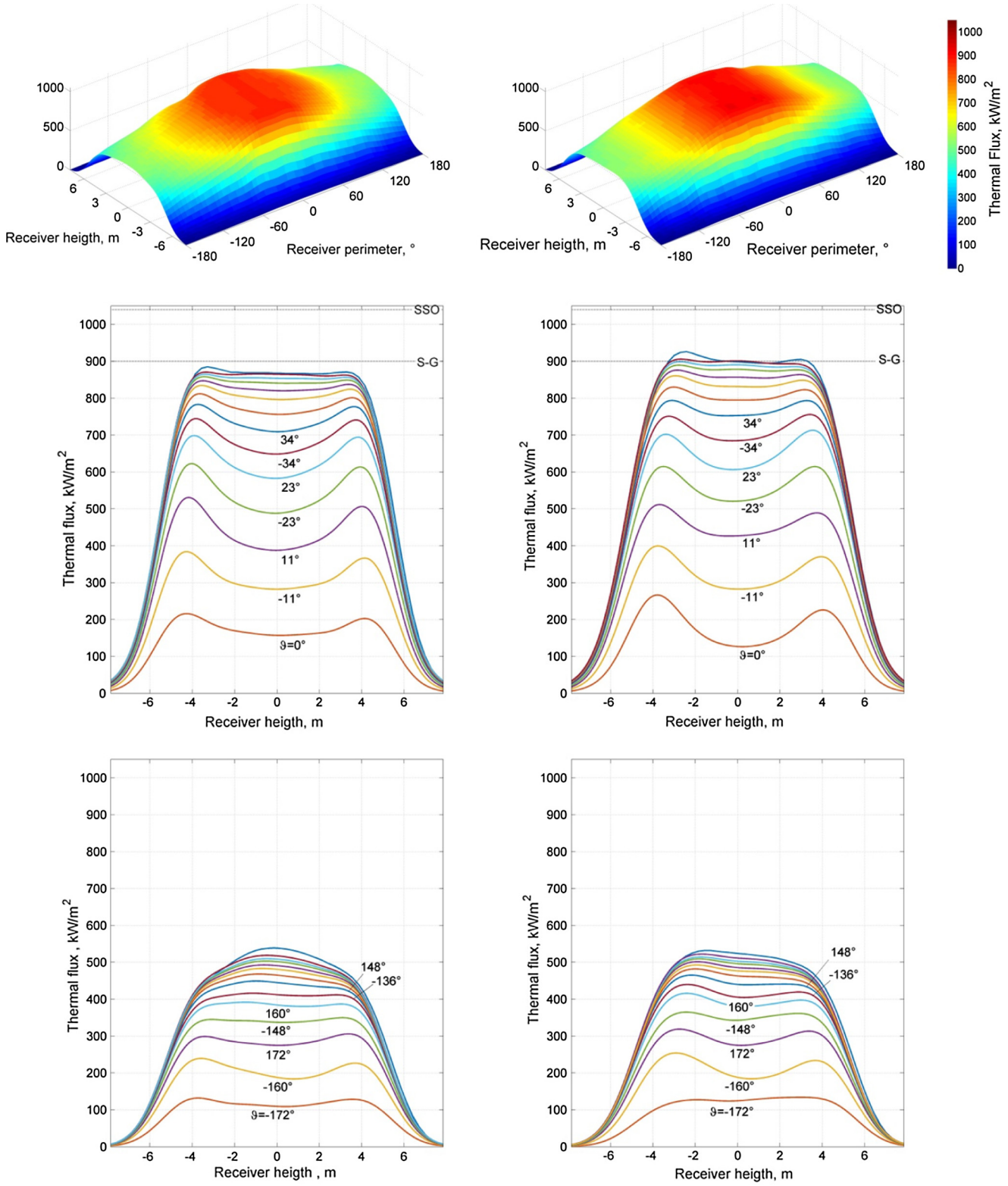

Fig. 10. Results for PSSO1 (left side) and PSSO2 (right side) aiming strategies: (top) Receiver 3-D, (middle) flux maps Flux profile at $\vartheta = 0°$ and $\vartheta = -174°$ (bottom).

In Fig. 10, the maps of heat flux are reported for both methods and it is possible to highlight that they are able to reduce the maximum heat flux compared to the REF case and results are similar to Sanchez Gonzales (PSSO1 slightly better, while PSSO2 slightly worse).

5.3. Explicit Overlap optimization (EO)

This approach aims to consider directly the cross-effects of neighbor sectors in the heat flux optimization of the most critical receiver vertical line.

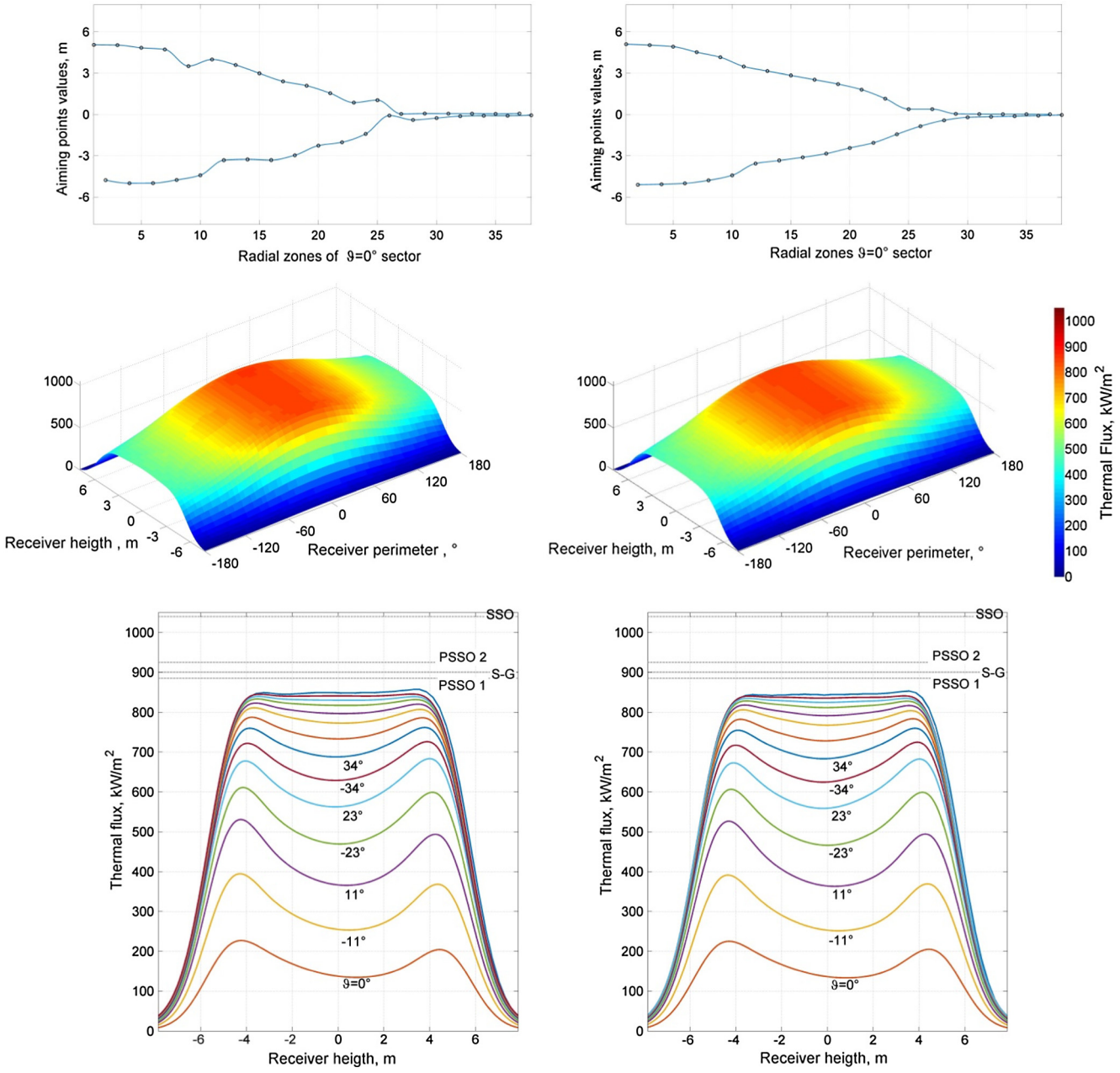

Fig. 11. Results for EO1 (left side) and EO2 (right side) aiming strategies: (top) y- pointing distance from the receiver center for the different radial zones, (middle) receiver 3-D Flux maps and (bottom) flux profile at $\vartheta = 0^{\circ}$.

In principle, all the heliostats with influence on the $\vartheta = 0^{\circ}$ receiver vertical line should be considered in the optimization but this approach leads to inaccurate results. Distant sectors (i.e.) have a limited contribution on the overall heat flux because the actual heat flux coming from these sectors on $\vartheta = 0^{\circ}$ receiver vertical line is a small portion of a larger solar projection. Neglecting this aspect entails two problems namely (i) high spillage losses and (ii) non-controllable heat flux profile in the other receiver portions. The first issue can be solved by keeping different lower and upper bounds for the pointing of each radial zone in each solar field sector and it requires additional Delsol simulations to set these parameters. The second one instead can be solved only with an iterative procedure: the optimization should be repeated for each receiver vertical line to find a new pointing for each radial zone. The final solution would be a compromise between the different optimal pointing with an increase of computational time and convergence issues.

Starting from these considerations and the symmetry of the heliostat field[5], a new aiming strategy based only on the

[5] The cross effects of two adjacent sectors are almost equal and it is reasonable to assume that the aiming strategy of all the sectors should be similar independently of the sun position and the receiver vertical line considered in the optimization.

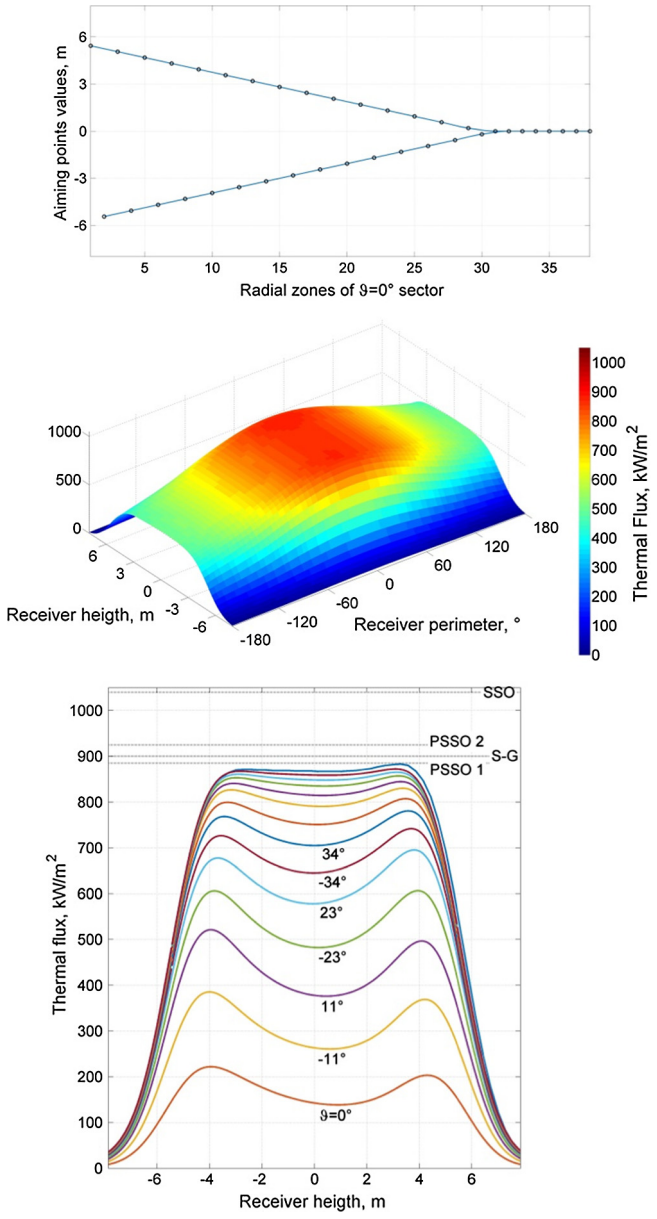

Fig. 12. Results for OOEA aiming strategy: (top) y- pointing distance from the receiver center for the different radial zones, (middle) receiver 3-D Flux map and (bottom) flux profile at $\vartheta = 0°$.

optimization of the 38 radial zones for the most critical solar field sector is proposed. This new strategy is called Explicit Overlap Optimization (EO).

This strategy requires 620 Delsol simulations in the pre-processing stage that is the number of radial zones which affect the heat flux of the $\vartheta = 0°$ receiver vertical line and it requires only one constraint: even radial zones point at the upper part of the receiver while the odd ones the opposite (EO1). The resulting optimized y-pointing for the $\vartheta = 0°$ solar field sector is reported in Fig. 11. The same aiming strategy is extended to all the other sectors and the y-pointing is imposed by scaling the aiming strategy plot for the actual number of radial zones in each sector. The interpolation of the optimized y-pointing of the $\vartheta = 0°$ sector is performed with the Piecewise Cubic Her-mite Interpolating Polynomial method.

Once the aim point for each one of the 38 radial zones is defined, the overlap effects on the $\vartheta = 0°$ receiver vertical line and the total heat flux is determined using the Gaus-sian functions obtained from the pre-processing stage. The total flux could also be calculated with Delsol with higher computational time.

The trend is almost symmetric since the radius of the solar images increases gradually moving toward the last radial zones.

This aiming strategy results in a very flat heat flux pro-file as reported in Fig. 11 demonstrating that the algorithm is now able to consider properly the overlap effects. In fact, the heat flux generated by the $\vartheta = 0°$ solar field sector presents two peaks at the receiver extremity in order to compensate the cross effects of the other sectors which are more pronounced at the center.

This result is the best one attainable with this approach, however one more strategy is investigated: it is based on the EO1 approach adding constraint of monotonicity for the two curves. This strategy named EO2 will take advantage of an easy interpolation for the sectors having a different number of radial zones. The result is presented in Fig. 11 and it is possible to note that there is a negligible difference in terms of heat flux peak reduction compared to EO1.

5.4. Overall optimization with empirical approach (OOEA)

The last strategy investigated, named overall optimization with empirical approach (OOEA) aims to further reduce the overall computational time introducing two assumptions: (i) the y-pointing is a linear function of the radial zone number and (ii) a symmetric pointing between the even and the odd radial zones. In this case only two optimization variables are considered namely the y- pointing distance from the receiver center of the first radial zones and the slope of the line. All the radial zones, after the intersection of the two lines, point to the equator of the receiver. Since there are just two optimization parameters,

Table 3
Summary of the investigated algorithms with their main features.

Features	Investigated algorithm					
	S-G	SSO	PSSO1	PSSO2	EO	OOEA
Approach	Sectorial	Sectorial	Sectorial	Sectorial	Global	Global
Flux calculation	Gauss approx.	Gauss approx.	Gauss approx.	Gauss approx.	Gauss approx.	Delsol
Cross-effects	No	No	Yes	Yes	Yes	Yes
Strategy Parametrization	No	No	No	No	Yes	Yes

Table 4
Reference case main characteristics.

	η optical (%)	Overall power (MW)	Peak flux (kW/m^2)	OF[a] (kW/m^2)
Reference case	68.3	196.3	2140	39,073

[a] See mathematical formulation in Section 5.1.

Table 5
Results for the different aiming strategies investigated at 0, 5 and 10% ΔSpillage.

		S-G	SSO	PSSO1	PSSO2	EO2	OOEA
ΔSpillage	%	≈0					
η optical	%	68.2	68.2	68.2	68.2	68.2	68.2
Overall power	MW	196.1	196.1	196.1	196.1	196.1	196.1
Peak flux	kW/m^2	900	1040	885	925	850	880
OF	kW/m^2	7685	10,642	7360	7482	6086	6790
Optimization time[a]	s	130	260	240	230	105	65
Pre-processing	s	130	130	130	130	80	/
Optimization	s	/	130	110	100	25	65
ΔSpillage	%	≈0.3					
η optical	%	68.0	68.0	68.0	68.0	68.0	68.0
Overall power	MW	195.5	195.5	195.5	195.5	195.5	195.5
Peak flux	kW/m^2	880	950	790	815	770	790
OF	kW/m^2	7471	8156	5080	4736	3854	4637
Optimization time	s	130	230	250	220	120	65
Pre-processing	s	130	130	130	130	80	/
Optimization	s	/	100	120	90	40	65
ΔSpillage	%	≈0.6					
η optical	%	67.8	67.8	67.8	67.8	67.8	67.8
Overall power	MW	194.9	194.9	194.9	194.9	194.9	194.9
Peak flux	kW/m^2	885	884	740	760	735	760
OF	kW/m^2	7669	6754	3960	3556	3032	3753
Optimization time	s	130	230	240	220	120	65
Pre-processing	s	130	130	130	130	80	/
Optimization	s	/	100	110	90	40	65

[a] Optimization time refers to an ×64 r2014b Matlab version, Intel core i3-4150 RAM 8 Gigabytes.

the flux calculations can be carried out using directly Delsol for the entire solar field. Therefore, this optimization approach does not require any pre-processing stage and consequently it allows reducing the computational time.

The heat flux peak reduction with OOEA approach is less marked than EO (880 vs. 850 kW/m^2) since the problem has more constraints and less degree of freedom, but a quite good result is attainable with a very short computational time (65 vs. 105 s) as shown in Fig. 12.

5.5. Summary of the proposed strategies

To sum up, several aiming point strategies were considered and their main features are summarized in Table 3.

6. Results

This section presents the results in terms of peak flux, objective function value and computational time for the different optimization approaches presented in this work. Results for the reference case and the different aiming strategies investigated at three ΔSpillage are reported in Tables 4 and 5.

Compared to the reference case, the peak flux and OF reductions for the investigated cases are of about 50/60% and 80% respectively with almost the same optical efficiency. The OF is representative of the difference between the actual flux distribution and the ideal case. Beside some particular cases, peak flux is as well representative of the optimization results. For example at 0% ΔSpillage, S-G has a lower peak flux compared to PSSO2 but it has a higher OF meaning that, even if peak flux on the hottest spot of the receiver is lower, the whole heat flux map is less uniform.

Increasing the ΔSpillage from 0% to 0.3% allows a further flux reduction of about 100 kW/m^2. This result is similar to a previous study carried out for a cavity receiver (Salomé et al., 2013). The implemented S-G approach is the only one for which the lowest peak flux and OF occur at 0.3% ΔSpillage. This is because S-G does not perform any optimization, but assigns the heliostat aiming points with a predetermined logic.

It can be noted that EO is the best optimization approach at any ΔSpillage investigated condition and it requires more computational time only than OOEA case. OOEA is the second approach in terms of OF and peak

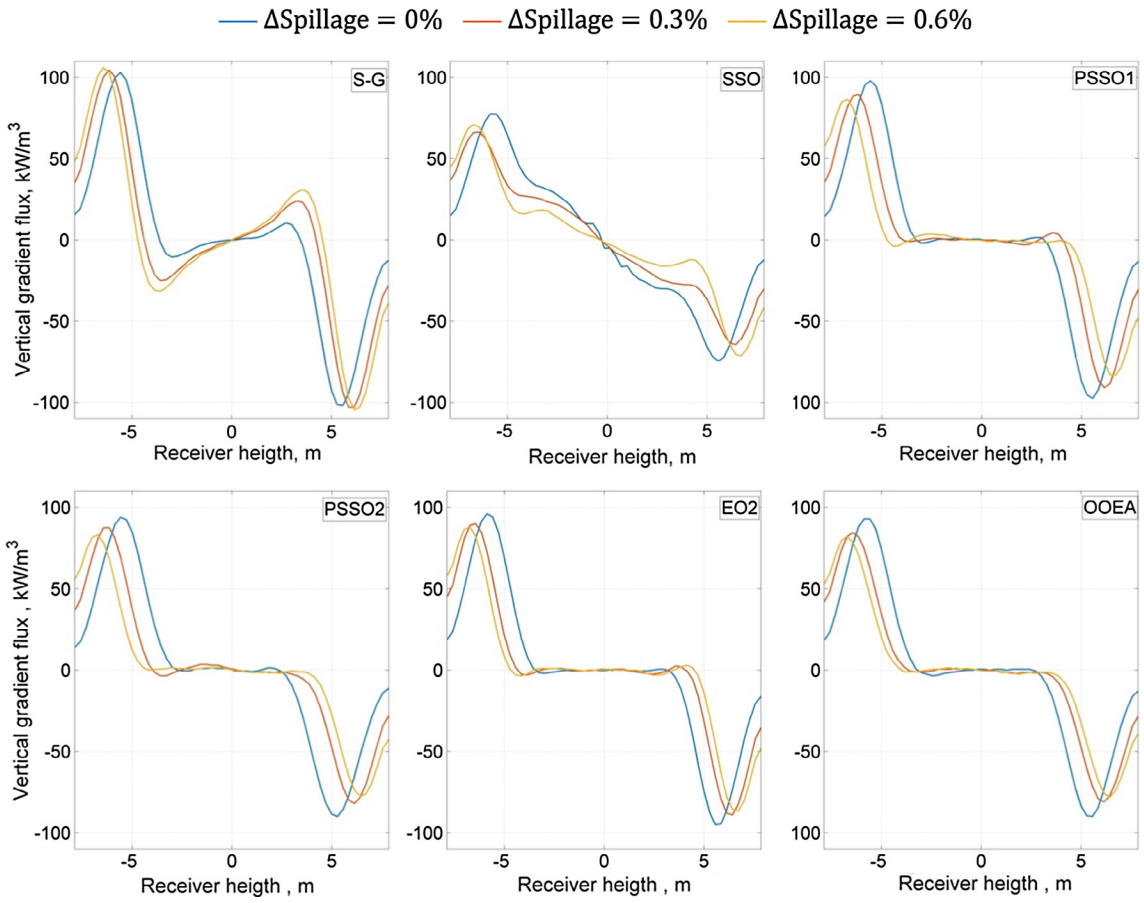

Fig. 13. Vertical gradient flux along the receiver at $\vartheta = 0°$ for the considered strategies.

flux at 0% and 0.3% ΔSpillage, while it performs less efficiently at 0.6% ΔSpillage. However it is always the quickest optimization approach.

Another aspect to be considered in the receiver design is the flux gradient along the height of the receiver. Gradients for investigated cases at different ΔSpillage are shown in Fig. 13. The case with lowest peak flux has the highest gradient at about −5/+5 m of receiver height. This is a consequence of the flat flux in the equator of the receiver.

S-G is the only one where a gradient inversion occurs. Finally, ΔSpillage increase has a limited impact on the gradient flux.

In order to demonstrate the validity of the proposed approach at any given solar conditions, the peak fluxes at different hours of the day (only afternoon is considered because of the solar field symmetry) and different days of the year at solar noon are presented in Fig. 14. The calculation are carried out for a ΔSpillage of 0.4% since it seems the best compromise between peak flux reduction and energy penalties. However, the same considerations can be also extended to the other considered cases[6].

[6] At extreme angles (dawn and dusk) the solar images becomes elliptical and the Gaussian approximation may introduce deviations up to 20% (Landman et al., 2016). This fact cannot be accounted here since Delsol is based on Gaussian convolution but the general conclusions are still valid.

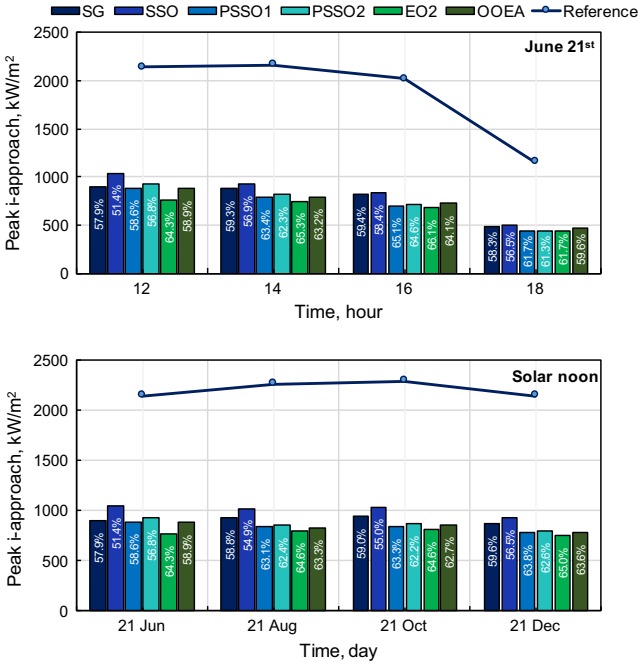

Fig. 14. Peak flux compared to the reference case at different hours of the day (top) on the June 21st and day of the year at solar noon (bottom). The white figures are the relative peak reductions for each case.

Results demonstrate that the peak reduction is between 57% and 66% in all cases. On June 21st, the highest reduction is achieved at 16 pm. With the single aim strategies (REF), the most critical day of the year is October 21st, while all the optimization strategies allow to achieve a constant heat flux at any day of the year. This supports the adoption of 21st of June at noon as reference condition. The most efficient approach is EO2 in all cases.

7. Sensitivity analysis

This section presents the impact of some assumptions on the results. In particular, two aspects will be analyzed in detail: heliostat errors and heliostat curvature. The analysis is performed for the two most promising approaches: EO2 and OOEA. As reported in the case study assumptions (see Table 1), all the calculations made in the previous sections were performed assuming for all the heliostats a focal length equal to the slant range (i.e. the number of curva-tures was set equal to the number of radial zones) and the error was equal to 0.75, 1.0 and 2.9 mrad for the heliostat angles, surface normal and reflected vector respectively.

Calculated efficiency and peak flux for different numbers of heliostats curvature are shown in Table 6. One curvature indicates that all the heliostats in the solar field have the same curvature (assumed as the average slant range), while 38 curvatures means that all the radial zone have a different curvature which coincides with the slant range.

With few number of curvatures (below six), the peak flux for the reference case reduces while the optical effi-ciency has limited variation. The optimized approach still gives benefits limiting the peak flux compared to the refer-ence case even though in relative terms the reduction is lower. Above eight curvatures, the impact on peak flux and optical efficiency can be considered negligible.

A similar sensitivity analysis has been conducted regarding the heliostats errors, analyzing in particular the impact of a larger (+50%) and a smaller error (−50%) on angles, surface normal and reflected values. The resulting peak flux and the optical efficiency for the reference case, the EO2 and the OOEA with maximum ΔSpillage = 0.4% are reported in Table 7.

The reference approach has an increase of the peak flux upon reducing the aiming errors because the heliostat aiming points get closer to the equator of the receiver; consequently the optical efficiency improves. On the other hand, the two proposed aiming strategies (EO2 and OOEA) show a different trend. With EO2, if the error decreases, the peak flux decreases and the optical efficiency increases because the actual aiming points are closer to the optimal ones. If the aiming error gets higher, the optical efficiency decreases since the spillage losses become more relevant; however, this negative effect has a positive impact on the peak flux which can decrease appreciably. The case with OOEA is equivalent to the EO2 in term of optical effi-ciency. However, due to the empirical approach, when the error is lowest (−50%) the peak flux slightly increases.

Table 6
Influence of assumed heliostat curvatures on the peak flux with the reference and OOEA strategies with Δ spillage $\approx$ 0.3%.

Number of curvatures (–)	Reference peak (kW/m^2)	OOEA peak (kW/m^2)	η reference (%)	η OOEA (%)
2	1800	1050	68.0	67.7
4	1970	880	68.2	67.9
6	2050	825	68.2	68.0
8	2080	795	68.2	68.0
10	2100	810	68.3	68.0
15	2120	805	68.3	68.0
38 (slant range)	2140	780	68.3	68.0

Table 7
Impact of assumed heliostat errors on peak flux for the reference case, EO2 and OOEA approach.

	Variation	Absolute (mrad)	Peak flux (kW/m^2)			η (%)		
			Reference	EO2	OOEA	Reference	EO2	OOEA
Heliostat angles	−50%	0.375	2240	760	800	68.5	68.3	68.3
	Default	0.75	2140	770	780	68.3	68.0	68.0
	50%	1.125	2000	770	755	67.8	67.4	67.4
Surface normal	−50%	0.5	2330	765	815	69.1	68.8	68.8
	Default	1	2140	770	780	68.3	68.0	68.0
	50%	1.5	1890	760	770	66.9	66.6	66.6
Reflected vectors	−50%	1.45	2630	770	800	70.8	70.5	70.5
	Default	2.9	2140	770	780	68.3	68.0	68.0
	50%	4.35	1660	740	755	64.2	63.9	63.9

8. Conclusions and future works

This paper compared different optimization approaches for the reduction of peak heat flux on central tower receiver. The optimization is carried out for a solar plant with an external receiver and a surround field located in Seville (Spain). The mathematical formulation is implemented in Matlab while the heliostat optical analysis is carried out in Delsol. Since solar field is constituted by thousands of heliostats, the optimization process is very complex. Therefore, different methods, based on branching the main optimization problem in simpler sub-problems, have been proposed to overcome this issue. The most efficient approaches were the ones that took into account the overlap of flux from neighbor heliostats: an optimization which considers each sector independently cannot be accurate since the overlapping effect distorts the independently optimized heat flux profile. The most efficient approach, among those proposed in this work, achieves, in reference conditions, a peak flux of about 800 kW/m^2 which is 15% lower than the best method proposed in literature (Sánchez-González and Santana, 2015b). A similar proof can be achieved at any solar position and for different assumptions on admissible spillage losses and heliostats errors. Increasing the spillage by 0.3% can reduce the heat fluxes of about 100 kW/m^2, while a spillage further increase will only penalize the optical efficiency without relevant advantages in terms of heat flux reduction. The gap between optimal strategy and S-G gets smaller while reducing the $\Delta Spillage$ but the optimized approach always allows for a peak flux reduction. A sensitivity analysis showed that the optimization approaches can work effi-ciently even with different assumptions on heliostat errors or number of curvatures.

The computational time is between one and three minutes on a commercial laptop for 2650 heliostats: therefore this optimization time can be reduced adopting high performance machine making the methods competitive for continuous monitoring of solar plants.

As drawback of the heat flux minimization, an increase of the heat flux gradient at the border of the receiver appears: therefore a detailed mechanical design and stress analysis should be carried out to determine the optimal design condition and perhaps reduce the receiver cost and thermal losses by shortening the receiver.

Next work will focus on the application of the optimized heat fluxes to a receiver thermal model to determine the impact on receiver temperatures and thermal efficiency and material stresses.

References

Abengoa, 2014. Khi Solar One [WWW Document]. URL <http://www.abengoasolar.com/web/en/nuestras_plantas/plantas_en_construccion/sudafrica/index.html>.

Augsburger, G., 2013. Thermo-economic optimisation of large solar tower power. École Polytechnique Fédérale de Lausanne.

Augsburger, G., Favrat, D., 2013. Modelling of the receiver transient flux distribution due to cloud passages on a solar tower thermal power plant. Sol. Energy 87, 42–52. http://dx.doi.org/10.1016/j.solener.2012.10.010.

Behar, O., Khellaf, A., Mohammedi, K., 2013. A review of studies on central receiver solar thermal power plants. Renew. Sustain. Energy Rev. 23, 12–39. http://dx.doi.org/10.1016/j.rser.2013.02.017. Besarati, S.M., Yogi Goswami, D., Stefanakos, E.K., 2014. Optimal heliostat aiming strategy for uniform distribution of heat flux on the receiver of a solar power tower plant. Energy Convers. Manage. 84, 234–243. http://dx.doi.org/10.1016/j.enconman.2014.04.030.

Boerema, N., Morrison, G., Taylor, R., Rosengarten, G., 2013. High temperature solar thermal central-receiver billboard design. Sol. Energy 97, 356–368. http://dx.doi.org/10.1016/j.solener.2013.09.008.

Buck, R., Teufel, E., 2009. Comparison and optimization of heliostat canting methods. J. Sol. Energy Eng. 131, 011001. http://dx.doi.org/10.1115/1.3027500.

Collado, F.J., 2009. Preliminary design of surrounding heliostat fields. Renew. Energy 34, 1359–1363. http://dx.doi.org/10.1016/j.renene.2008.09.003.

Collado, F.J., Guallar, J., 2013. A review of optimized design layouts for solar power tower plants with campo code. Renew. Sustain. Energy Rev. 20, 142–154. http://dx.doi.org/10.1016/j.rser.2012.11.076.

CSP world website [WWW Document], 2014. URL <http://www.csp-world.com/cspworldmap>.

CSP-Alliance, 2012. The economic and reliability benefits of CSP with thermal energy storage: recent studies and research needs. URL <http://www.csp-alliance.org/wp-content/uploads/2014/10/The_Economic_and_Reliability_Benefits_of_CSP_with_Thermal_Storage-2014_10_15-FINAL.pdf>.

Delaquil, P., Kelly, B., Lessley, R., 1991. Solar one conversion project. Sol. Energy Mater. 24, 151–161. http://dx.doi.org/10.1016/0165-1633(91)90055-P.

Delhom, P., Hommon, M., 2012. Simulating the Value of Concentrating Solar Power with Thermal Energy Storage in a Production Cost Model. Golden, Colorado (US).

Delsol web page [WWW Document], 2014. URL <http://energy.sandia.gov/?page_id=6530>.

Garcia, P., Ferriere, A., Bezian, J., 2008. Code for solar flux calculation dedicated to central receiver system application: a comparative review. Sol. Energy 82, 189–197.

GarcÍa-MartÍn, F.J., Berenguel, M., Valverde, M., Camacho, E.F., 1999. Heuristic knowledge-based heliostat field control for the optimization of the temperature distribution in a volumetric. Sol. Energy 66, 355–369. http://dx.doi.org/10.1016/S0038-092X(99)00024-9.

Gemasolar [WWW Document], 2014. URL <http://www.torresolenergy.com/TORRESOL/gemasolar- plant/en>.

Ho, C., 2008. Software and codes for analysis of concentrating solar power technologies. Albuquerque, NM, US.

IEA, 2011. Solar Energy perspectives. Paris. URL <http://www.iea.org/publications/freepublications/publication/solar_energy_perspectives2011.pdf>.

Ivanpah plant [WWW Document], 2014. URL <http://ivanpahsolar.com/>.

Kistler, B., 1986. A user's manual for DELSOL3: a computer code for calculating the optical performance and optimal system design for solar thermal central receiver plants. URL <http://prod.sandia.gov/techlib/access-control.cgi/1986/868018.pdf>.

Landman, W., Gauché, P., 2014. Influence of canting mechanism and facet profile on heliostat field performance. Energy Proc. 49, 126–135. http://dx.doi.org/10.1016/j.egypro.2014.03.014.

Landman, W.A., Grobler, A., Gauché, P., Dinter, F., 2016. Incidence angle effects on circular Gaussian flux density distributions for heliostat imaging. Sol. Energy 126, 156–167. http://dx.doi.org/ 10.1016/j.solener.2015.12.008.

Lipps, F., Vant-Hull, L., 1978. A cellwise method for the optimization of large central receiver systems. Sol. Energy 20, 505–516.

Lipps, F., Pitman, C., Vant-Hull, L., 1985. Combined collector-receiver optimization for central receiver systems using RCELL. In:
ASME-ASES Meeting. Knoxvill, Tn, March 2985.
Pacheco, J., 2002. Final test and evaluation results from the solar two project. Albuquerque, NM, US. URL <http://prod.sandia.gov/tech-lib/access-control.cgi/2002/020120.pdf>.
REN21, 2013. Renewable 2013 Global status report. Paris. URL <http://www.ren21.net/Portals/0/documents/Resources/GSR/2013/
GSR2013_lowres.pdf>.
Rodríguez-Sánchez, M.R., Marugan-Cruz, C., Acosta-Iborra, A., Santana, D., 2014a. Comparison of simplified heat transfer models and CFD simulations for molten salt external receiver. Appl. Therm. Eng. 73, 991–1003. http://dx.doi.org/10.1016/j.applthermaleng.2014. 08.072.

Rodríguez-Sánchez, M.R., Soria-Verdugo, A., Almendros-Ibáñez, J.A., Acosta-Iborra, A., Santana, D., 2014b. Thermal design guidelines of solar power towers. Appl. Therm. Eng. 63, 428–438. http://dx.doi.org/10.1016/j.applthermaleng.2013.11.014.
Salomé, A., Chhel, F., Flamant, G., Ferrière, A., Thiery, F., 2013. Control of the flux distribution on a solar tower receiver using an optimized aiming point strategy: application to THEMIS solar tower. Sol. Energy 94, 352–366. http://dx.doi.org/10.1016/j.solener.2013.02.025.
Sanchez, M., Romero, M., 2006. Methodology for generation of heliostat field layout in central receiver systems based on yearly normalized energy surfaces. Sol. Energy 80, 861–874.
Sánchez-González, A., Santana, D., 2015a. Solar flux distribution on central receivers: a projection method from analytic function. Renew. Energy 74, 576–587. http://dx.doi.org/10.1016/j.renene.2014.08.016.
Sener [WWW Document], 2014. URL <http://www.sener.es/sener-magazine/en>.
Solucar, 2006. 10 MW Solar Thermal Power Plant for Southern Spain. URL <http://ec.europa.eu/energy/res/sectors/doc/csp/ps10_final_report.pdf>.
SunShot website [WWW Document], 2014. URL <http://energy.gov/eere/sunshot/sunshot-initiative> (accessed 1.1.16).
Vant-Hull, L., Izygon, M., 2003. Guidelines to central receiver system heliostat field optimization. Adv. Sol. Energy, 15.
Vant-Hull, L.L., Izygon, M.E., Pitman, C.L., 1996. Real time computation and control of solar flux density on a central receiver (solar two), (protection against excess flux density). In: Campbell-Howe, R., Wilkins-Crowder, B. (Eds.), Solar 96 – Proceedings of the 1996 Annual Conference. American Solar Energy Society, Asheville NC, pp. 88–94.

Wright, S., Scott, D., Haddow, J., Rosen, M., 2000. The upper limit to solar energy conversion. 35th Intersoc. Energy Convers. Eng. Conf. http://dx.doi.org/10.2514/6.2000-2861.
Yu, Q., Wang, Z., Xu, E., 2014. Analysis and improvement of solar flux distribution inside a cavity receiver based on multi-focal points of heliostat field. Appl. Energy 136, 417–430. http://dx.doi.org/10.1016/j.apenergy.2014.09.008.